PAPER

Check for updates

Unprecedented iron-assisted room temperature synthesis of AgCN using acetonitrile†

Nand Kishor Gour, [ID] [a] Manash J. Baruah, [ID] [b] Biraj Das [ID] *[c] and Mukesh Sharma [ID] *[d]

A straightforward and convenient approach for producing AgCN at room temperature using acetonitrile as a source has been developed, employing various iron salts. To date, there have been no prior studies documenting the synthesis of AgCN by cleaving the C–CN bond in acetonitrile with the use of iron salts. The resulting highly crystalline material was subjected to characterization through XRD and FT-IR analysis. Additionally, the same process was used for C–CN bond breaking using Ag_2S or *via* the formation of an AgS_xO_y composite. Consequently, this report is primarily dedicated to exploring the efficacy of different iron salts in breaking the C–CN bond in CH_3CN. A theoretical investigation of the proposed experimental scheme has also been performed to confer the feasibility of the reaction.

Introduction

The use of non-toxic cyanide sources or cyanation agents has remained a major problem for organic chemists and the chemical industry due to its high toxicity and complex methodologies.[1–4] Starting from the famous work on potassium ferrocyanide with sulfuric acid by the Swedish scientist Carl Wilhelm Scheele, numerous methodologies have been employed to date for the replacement of toxic HCN, NaCN, KCN, DDQ, malononitriles, *etc.* as a source of cyanating agents.[1] Of particular interest is the breaking of C–CN bonds in acetonitrile (CH_3CN) due to its potential applications in organic synthesis and its role as a source of cyanide ions (CN^-).[2] However, the high thermodynamic stability and bond dissociation energy of the C–CN bond in CH_3CN limit its use as a green source of cyanide ions.[5–7] To address this, various metal complexes have been developed to activate C–C bonds in aryl and alkyl cyanides.[2,8,9] Henceforth, researchers have shifted their attention to the cleavage of unreactive bonds like C–C, C–O, C–N, and C–Cl particularly in the context of organic compound synthesis.[10]

Taw *et al.* conducted experiments wherein they observed the displacement of dichloromethane by PhCN, leading to the formation of $[Cp*(PMe_3)Rh(R)(CNSiPh_3)]^+BAr_4^-$ when Ph_3SiH was employed as a reactant.[2] Subsequently, this intermediate transformed into $[Cp*(PMe_3)Rh(Me)(CH_2Cl_2)]^+BAr_4^-$. Additionally, acetonitrile cleavage was accomplished through a photoreaction utilizing the $Cp(CO)_2Fe(SiMe_3)$ complex forming $CpL_2Fe(CN)$.[8] In a separate study, Gou *et al.* reported the cleavage of the C–CN bond within CH_3CN during the formation of an Ag(I) complex under solvothermal conditions.[9] Furthermore, Zou *et al.* employed a photo-assisted process to produce metal cyanides by reacting various transition metal nitrate salts (Ag^+, Zn^{2+}, Yb^{2+}, and Ni^{2+}) with CH_3CN.[5] In a separate study, Okabayashi *et al.* demonstrated the formation of monomeric AgCN and AuCN through the cleavage of the C–CN bond in CH_3CN in the gas phase, utilizing a sputtering reaction involving Ag sheet and CH_3CN.[11]

In recent research endeavors, a range of vanadium-based materials were designed for the direct synthesis of AgCN from CH_3CN.[12–14] However, it is worth noting that, to the best of our knowledge, the synthesis of AgCN *via* the C–CN bond cleavage in CH_3CN using iron salts has not been documented in existing literature. Due to the rapid and cost-effective synthesis of pure AgCN using iron salts, we believe this process holds great potential for various industrial and laboratory applications, as it eliminates the need for toxic alkali cyanides such as NaCN and KCN. Consequently, this report aims to investigate the potential of various iron salts in catalyzing the cleavage of the C–CN bond utilizing CH_3CN as the substrate.

Experimental section

Synthesis of silver cyanide (AgCN) from silver nitrate ($AgNO_3$)

To carry out the reaction, 100 mg of iron nitrate $Fe(NO_3)_3$ was dissolved in a 100 mL round-bottom flask containing 10 mL of CH_3CN. The reaction mixture was then stirred at room

[a]Department of Chemical Sciences, Tezpur University, Napaam, Tezpur – 784028, Assam, India. E-mail: nkgour1@tezu.ernet.in
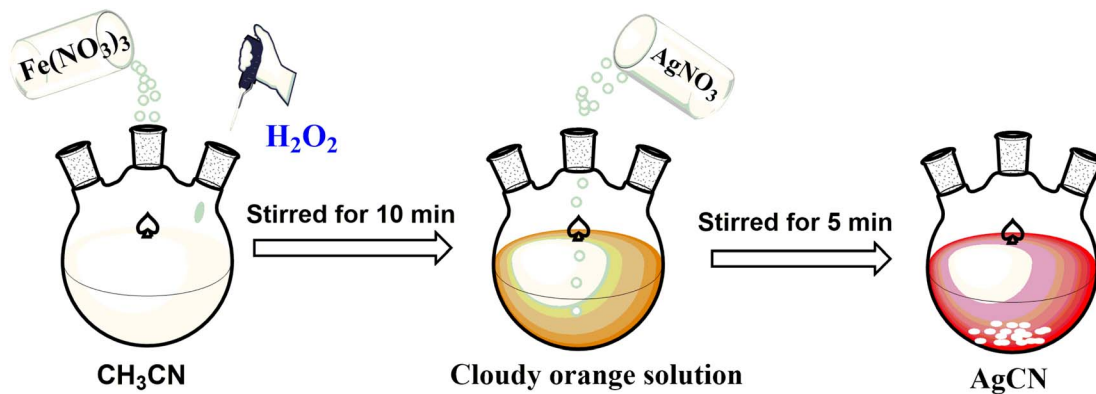
[b]Department of Chemistry, D. C. B. Girls College, Jorhat, Assam, 785001, India. E-mail: manashjbom@gmail.com

[c]Department of Chemistry, D. D. R. College, Chabua, Dibrugarh, Assam, 786184, India. E-mail: birajdaschm@gmail.com

[d]Department of Chemistry, Suren Das College, Hajo, Kamrup, Assam, 781102, India. E-mail: mcotton233@gmail.com

Scheme 1 Schematic representation for the formation of AgCN.

temperature for 10 min after adding 2 mL of H_2O_2. Upon the formation of a red solution, 100 mg of $AgNO_3$ was introduced to the solution and stirred for an additional 5 minutes, resulting in the formation of a white precipitate of AgCN. The AgCN material was thoroughly washed with distilled water and subsequently dried in an oven at 100 °C, Scheme 1.

Results and discussion

The white precipitate obtained was subjected to XRD and FT-IR analysis as depicted in Fig. 1. The XRD pattern revealed sharp and well-defined peaks at 2θ values of 24, 29.7, 38.2, 49.2, 52.7, 58.4, and 61.3, which corresponded to the presence of crystalline AgCN material, Fig. 1a.[14,15] Markedly, no additional peaks indicative of Ag_2O or Ag NPs were observed in the XRD pattern which circuitously supports the highly crystalline nature of the formed AgCN.[16,17] In the FT-IR analysis, the presence of a strong vibrational band at 2140 cm^{-1} and a weak band at 2163 cm^{-1} confirmed the existence of the $-C\equiv N$ bond.[18,19] Additionally, the observation of a strong band at 476 cm^{-1} indicated the presence of a Ag–C bond, Fig. 1b.[12–14]

To optimize the synthesis of AgCN, we conducted experiments in which we varied the quantity of H_2O_2 while maintaining all other reaction parameters constant. Initially, when we employed 0.5 mL of H_2O_2 alongside 100 mg of $Fe(NO_3)_3$ and 10 mL of CH_3CN, we did not observe the formation of AgCN precipitate. Consequently, we increased the amount of H_2O_2 to 1 mL, resulting in the formation of 56 mg of AgCN. To determine the ideal quantity of H_2O_2 needed for 100 mg of $Fe(NO_3)_3$, we conducted trials with varying amounts of H_2O_2, ranging up to 3 mL, as detailed in Table 1. Fortunately, we found that 2 mL of H_2O_2 yielded the highest conversion of

Table 1 Optimized condition for the formation of AgCN with 100 mg of $AgNO_3$ with respect to different Fe-catalysts

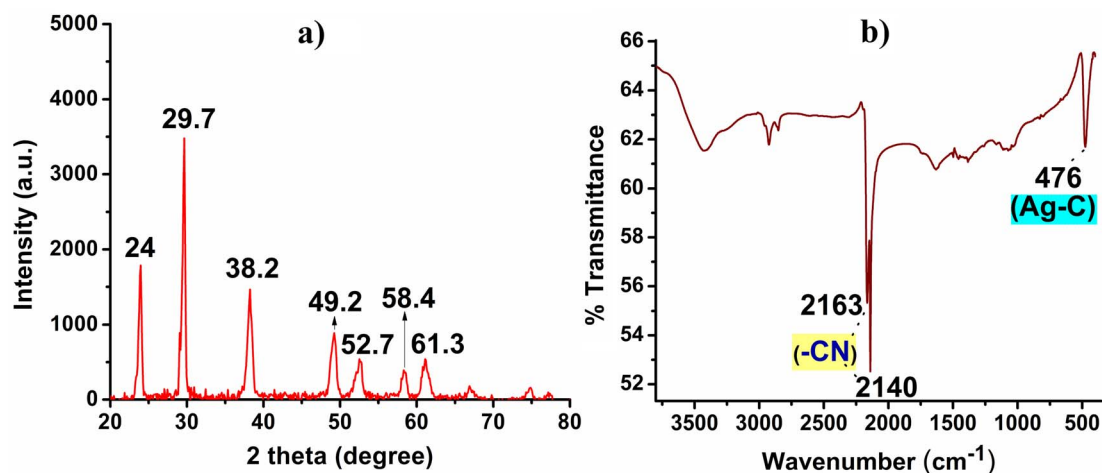| S. no.	$Fe(NO_3)_3/FeSO_4\cdot 7H_2O$ (100 mg)	CH_3CN (mL)	H_2O_2 (mL)	AgCN (mg)
1	$Fe(NO_3)_3$	10	0.5	0
2	$Fe(NO_3)_3$	10	1	56
3	$Fe(NO_3)_3$	10	1.5	64
4	$Fe(NO_3)_3$	10	2	75
5	$Fe(NO_3)_3$	10	2.5	76
6	$Fe(NO_3)_3$	10	3	76
7	$FeSO_4\cdot 7H_2O$	10	2	48

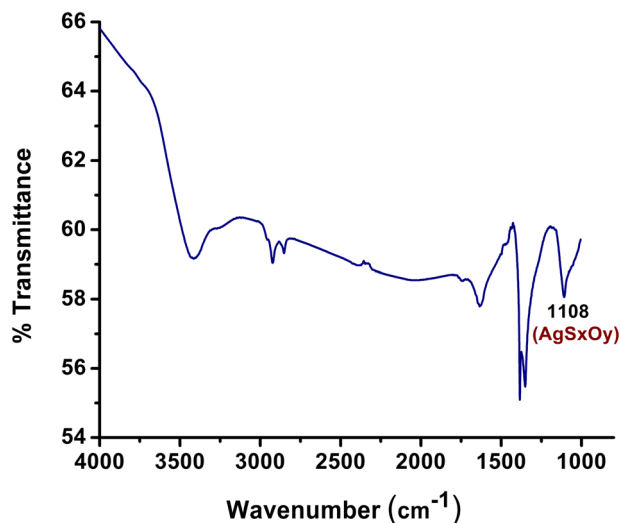**Fig. 1** (a) XRD pattern and (b) FT-IR spectra of the synthesized AgCN.

Fig. 2 FT-IR spectra of the synthesized composites.

AgNO$_3$ to AgCN, making it the optimal condition. Further increases in the amount of H$_2$O$_2$ did not enhance AgCN formation. Therefore, we concluded that the combination of 2 mL of H$_2$O$_2$, 100 mg of Fe(NO$_3$)$_3$, and 10 mL of CH$_3$CN represented the optimum reaction conditions.

To delve deeper into the reaction, we carried out additional investigations where we substituted iron nitrate Fe(NO$_3$)$_3$ with alternative iron salts while keeping the same reaction conditions. Specifically, we used ferrous sulfate (FeSO$_4$·7H$_2$O) as the iron salts in this experiment. Intriguingly, we observed the formation

of AgCN through the cleavage of CH$_3$CN with iron salts. However, there were subtle distinctions in their reactivity and outcomes when compared to the results obtained with Fe(NO$_3$)$_3$, which are summarized in Table 1. The red solution (Scheme 1) underwent recycling for up to three successive rounds in the cyanide extraction process, consistently exhibiting comparable activity and leading to the generation of silver cyanide (AgCN).

Silver sulfide (Ag$_2$S) ores play a vital role in global silver production and the extraction of silver from these ores is imperative to satisfy the demand for this precious metal.[20] The process of obtaining silver from Ag$_2$S ores can be financially sound, given that these ores frequently contain substantial silver content. This contributes to the revenue of mining companies and has a positive impact on both local and national economies.[14–16] Recognizing the substantial demand for silver extraction from Ag$_2$S ore, we endeavored to reproduce the same reaction under standard conditions, following our successful synthesis of AgCN using AgNO$_3$. Unfortunately, we did not observe the formation of AgCN in this instance. Given that Ag$_2$S is highly insoluble in both acids and organic solvents, we proposed that AgS$_x$O$_y$ material, which is soluble in hydrogen peroxide, might play a role in the reaction.[20] To investigate this hypothesis, we synthesized a composite of Ag$_2$S and Fe(NO$_3$)$_3$ by gradually introducing H$_2$O$_2$. The FT-IR analysis of this composite revealed a prominent band at 1108 cm^{-1}, indicating the transformation of Ag$_2$S into AgS$_x$O$_y$, Fig. 2.[14,21] Subsequently, when we added this synthesized composite to a mixture of CH$_3$CN and H$_2$O$_2$ at room temperature, AgCN was formed. To obtain pure AgCN, we washed the resulting sample with an aqueous solution of oxalic acid.
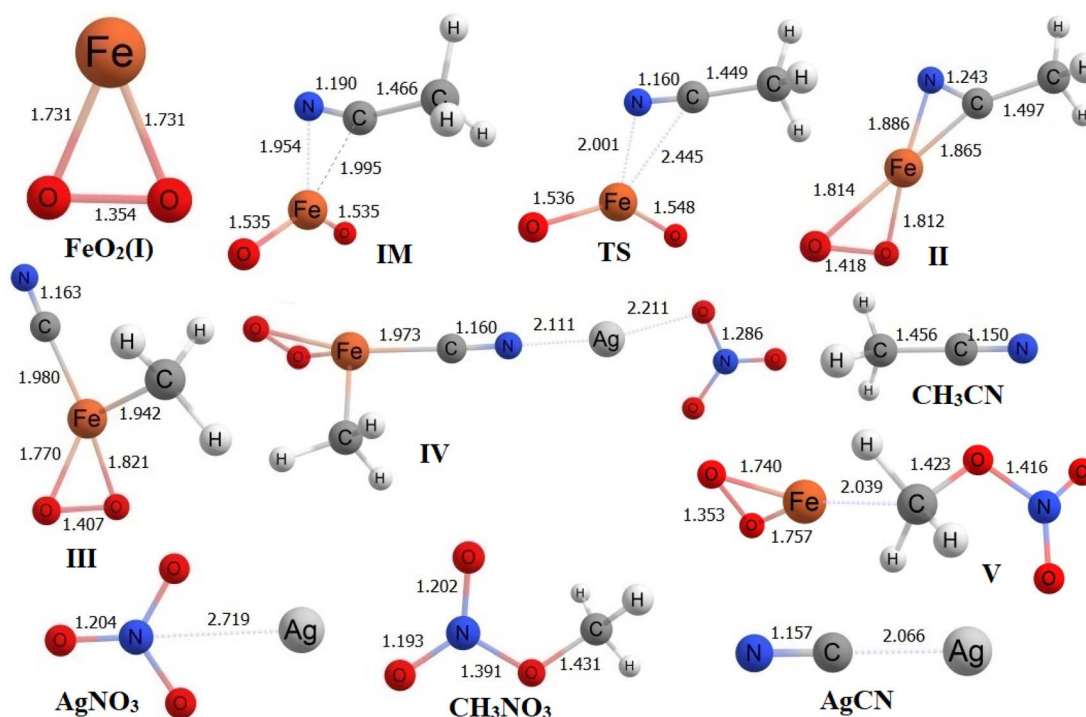

Fig. 3 Optimized geometries of all species at ωB97XD/6-311++G(d,p)/LANL2DZ level of theory.

Table 2 Standard enthalpy and Gibbs free energy changes (in kcal mol^{-1}) of reaction steps at ωB97XD/6-311++G(d,p)/LANL2DZ level of theory

Reaction steps	$\Delta_r H^o$	$\Delta_r G^o$
FeO$_2$ (I) + CH$_3$CN $\rightarrow$ IM	-85.96	-74.77
IM $\rightarrow$ TS	4.38	3.86
TS $\rightarrow$ II	-25.68	-25.87
II $\rightarrow$ III	-6.35	-7.29
III + AgNO$_3$ $\rightarrow$ IV	-49.72	-41.79
IV $\rightarrow$ V + AgCN	172.12	166.31
V $\rightarrow$ FeO$_2$+ AgCN + CH$_3$NO$_3$	14.35	3.38

Theoretical investigation

Electronic structures. The electronic structures of all stable species, intermediates (IM), and transition states (TS) are depicted in Fig. 3. Additionally, selected bond lengths (in Å) are presented in the same figure. In the optimized structure of FeO$_2$ (I), both Fe–O bonds exhibit an equal length of 1.731 Å, while the O–O distance measures 1.354 Å. Moving forward, FeO$_2$ (I) undergoes a reaction with CH$_3$CN to generate structure II through an intermediate (IM) and transition state (TS). In the IM structure, the bond distances between the C atom and N atom of CH$_3$CN with respect to the Fe atom of FeO$_2$ are 1.995 Å and 1.954 Å, respectively. In the TS, these bond distances
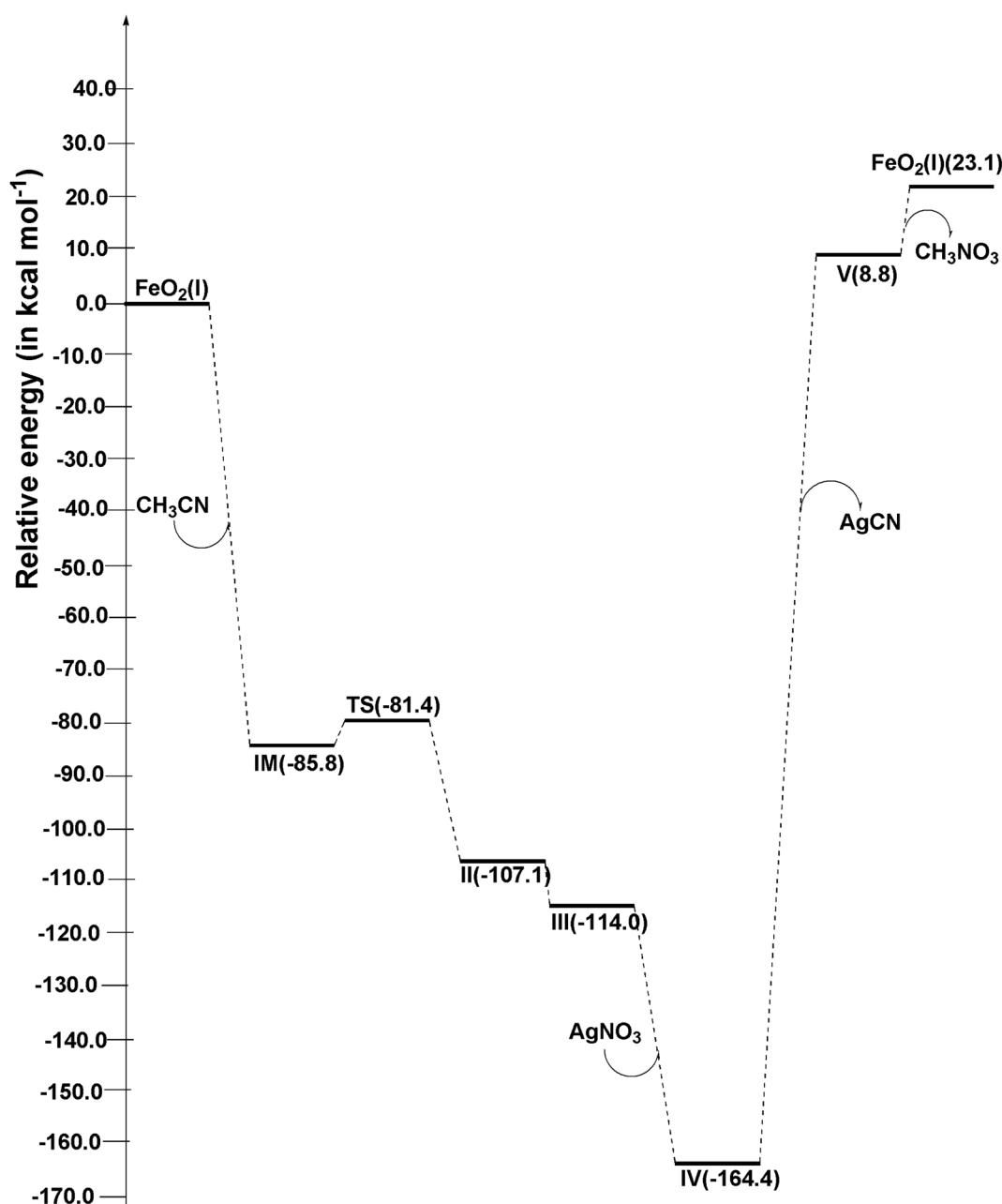

Fig. 4 Potential energy diagram of proposed reaction at ωB97XD/6-311++G(d,p)/LANL2DZ level of theory.

slightly increase and are measured at 2.445 Å and 2.001 Å, respectively, for the Fe atom of FeO_2. Notably, the C–C bond in CH_3CN within the TS decreases by approximately 0.327 Å (or roughly 22.6%) compared to the C–C bond in the IM structure.

Within structure II, the bond distances between the C atom and N atom of CH_3CN with the Fe atom of FeO_2 are 1.865 Å and 1.886 Å, respectively. To analyze the transformation from structure I to structure II, an IRC calculation was conducted. The IRC plot confirms that this TS effectively connects structures I and II along a reaction coordinate. In the transition from structure II to structure III, the CH_3 group in CH_3CN migrates toward the Fe atom, forming a bond at a distance of 1.942 Å. Simultaneously, the C atom of CN forms a bond with the Fe atom at a distance of 1.980 Å. In the subsequent step, $AgNO_3$ is introduced to structure III, and during the conversion to structure IV, the distance between the N atom of CN in structure IV and the Ag atom of $AgNO_3$ is measured at 2.111 Å. Meanwhile, the distance between the C atom of CN and the Fe atom is 1.973 Å. As the process proceeds from structure IV to structure V, AgCN is removed from structure IV to yield structure V. In structure V, the Fe–C and C–O distances are found to be 2.039 Å and 1.423 Å, respectively. Finally, in the last step, CH_3NO_3 is entirely desorbed from structure V, leading to the reformation of structure I.

Thermochemistry of the reaction

Thermo-chemical data, including total energy (E_0), enthalpy (H), and Gibbs's free energy (G), for all the species were determined through frequency calculations, and these values can be found in Table S3.† We calculated the enthalpy of the reaction ($\Delta_r H^o$) and Gibbs's free energy ($\Delta_r G^o$) for each step in the process illustrated in Fig. 3, and these values are provided in Table 2.

In the transition from FeO_2 (I) + CH_3CN to IM, both $\Delta_r H^o$ and $\Delta_r G^o$ exhibit negative values, indicating that this step is exothermic ($\Delta_r H^o < 0$) and spontaneous ($\Delta_r G^o < 0$) at room temperature. However, the subsequent step is slightly endothermic and non-spontaneous. The following three steps are characterized as exothermic and spontaneous processes. During the transformation from structure IV to structure V, which involves the removal of AgCN and requires an input of energy, this step is highly endothermic and non-spontaneous. Finally, in the last step where structure V converts back into structure I and CH_3NO_3, we also observe a slightly endothermic and non-spontaneous behavior.

Energy profile diagram

Using the absolute total energy data for all the species from Table S3,† we have determined the relative energies of these species for FeO_2 and explored their positions on the potential energy surface (PES), as depicted in Fig. 4. It is evident from Fig. 4 that, in addition to CH_3CN within FeO_2 (I), an intermediate (IM) structure is formed, resulting in a decrease in energy by 85.8 kcal mol^{-1}. Subsequently, this IM transforms into Structure II through a transition state (TS) structure, with an energy barrier of 4.4 kcal mol^{-1} relative to IM. The energy of structure II is measured at −25.7 kcal mol^{-1}. Moving forward, the energy of

structure III decreases further by −6.9 kcal mol^{-1} relative to structure II. In the next step, the introduction of $AgNO_3$ to structure III leads to a further decrease in the energy of structure IV relative to structure III, amounting to −50.4 kcal mol^{-1}. Following this, AgCN is eliminated from structure IV, forming structure V. This step necessitates an input of energy equal to 173.2 kcal mol^{-1}. Finally, structure V undergoes a conversion into FeO_2 (I) with the elimination of CH_3NO_3. This final step also requires an input of 14.3 kcal mol^{-1} relative to structure V.

Catalytic study

To see the efficacy and reactivity of the freshly synthesized AgCN, the material was employed for the dye degradation process and the details of compared results with the commercially available AgCN are provided in Fig. S1.† Upon investigation, it was determined that the synthesized AgCN exhibited greater reactivity compared to its commercially available counterpart.

Conclusions

This report presents a straightforward and efficient method for synthesizing AgCN using acetonitrile as a cyanide source at room temperature. What sets our work apart is the use of various iron salts, as there is no prior research demonstrating the synthesis of AgCN through the cleavage of the C–CN bond in acetonitrile with iron salts. Our study primarily focuses on investigating the potential of different iron salts to promote the cleavage of the C–CN bond in CH_3CN for AgCN synthesis. Through theoretical analysis, we delve into the thermochemistry of all the involved steps, thereby discussing the feasibility of the reaction. We anticipate that this supplementary theoretical exploration will contribute to raising the quality of the experimental investigation. The freshly synthesized AgCN material showcased enhanced reactivity in the dye degradation process compared to its commercially available counterpart underlining the uncompromised reactivity of the freshly synthesized AgCN.

Author contributions

Dr Gour conducted all the theoretical calculations for the experiment and provided insights into result interpretation. Dr Baruah processed the experimental data, conducted analysis, drafted the manuscript, and created the figures. Dr Sharma and Dr Das conceived and devised the experiments, contributed to the result analysis, writing, reviewing, and editing of the final manuscript. All authors engaged in result discussions and collaborated on the final manuscript.

Conflicts of interest

The authors declare no competing financial interest.

Acknowledgements

Notes and references

1 A. M. Nauth and T. Opatz, *Org. Biomol. Chem.*, 2019, **17**, 11–23.

2 F. L. Taw, P. S. White, R. G. Bergman and M. Brookhart, *J. Am. Chem. Soc.*, 2002, **124**, 4192–4193.

3 T. Ooi, Y. Uematsu and K. Maruoka, *J. Am. Chem. Soc.*, 2006, **128**, 2548–2549.

4 J. Schörgenhumer and M. Waser, *Org. Chem. Front.*, 2016, **3**, 1535–1540.

5 S. Zou, R. Li, H. Kobayashi, J. Liu and J. Fan, *Chem. Commun.*, 2013, **49**, 1906–1908.

6 Y. Zhu, M. Zhao, W. Lu, L. Li and Z. Shen, *Org. Lett.*, 2015, **17**, 2602–2605.

7 M. Tobisu and N. Chatani, *Chem. Soc. Rev.*, 2008, **37**, 300–307.

8 H. Nakazawa, T. Kawasaki, K. Miyoshi, C. H. Suresh and N. Koga, *Organometallics*, 2004, **23**, 117–126.

9 L. R. Guo, S. S. Bao, Y. Z. Li and L. M. Zheng, *Chem. Commun.*, 2009, **20**, 2893–2895.

10 K. Fukumoto, T. Oya, M. Itazaki and H. Nakazawa, *J. Am. Chem. Soc.*, 2009, **131**, 38–39.

11 T. Okabayashi, E. Y. Okabayashi, F. Koto, T. Ishida and M. Tanimoto, *J. Am. Chem. Soc.*, 2009, **131**, 11712–11718.

12 B. Das, M. Sharma, C. Kashyap, A. K. Guha, A. Hazarika and K. K. Bania, *Appl. Catal.*, 2018, **568**, 191–201.

13 B. Das, M. Sharma, M. J. Baruah, K. K. Borah and K. K. Bania, *Inorg. Chim. Acta*, 2019, **498**, 119160.

14 G. A. Bowmaker, B. J. Kennedy and J. C. Reid, *Inorg. Chem.*, 1998, **37**, 3968–3974.

15 Y. J. Lu, D. Janmanchi, T. Natarajan, Z. H. Lin, W. H. Wanna, I. J. Hsu, D. L. M. Tzou, T. Ayalew Abay and S. S. F. Yu, *ChemCatChem*, 2022, **14**, e202200030.

16 J. Ren and Y. Zhu, *RSC Adv.*, 2020, **10**, 6114–6120.

17 X. Wei, F. Cheng, Y. Yao, X. Yi, B. Wei, H. Li, Y. Wu and J. He, *RSC Adv.*, 2021, **11**, 18417–18422.

18 M. C. Ríos, N. F. Bravo, C. C. Sánchez and J. Portilla, *RSC Adv.*, 2021, **11**, 34206–34234.

19 G. Deschênes, J. Rajala, A. R. Pratt, H. Guo, M. Fulton and S. Mortazavi, *Min., Metall., Explor.*, 2011, **28**, 37–42.

20 H. Jiang, F. Xie and D. B. Dreisinger, *Hydrometallurgy*, 2015, **158**, 149–156.

21 K. Nakamoto, *Infrared and Raman Spectra of Inorganic and Coordination Compounds, Part B*, John Wiley & Sons, NY, 5th edn, 1997.